COMPONENT PART NOTICE

THIS PAPER IS A COMPONENT PART OF THE FOLLOWING COMPILATION REPORT:

(TITLE): Proceedings of the International Conference on the Performance of Off-Road Vehicles and Machines (8th) Volume 1 Held at Cambridge, England on August 5-11, 1984

(SOURCE): International Society for Terrain-Vehicle Systems

TO ORDER THE COMPLETE COMPILATION REPORT USE AD-148 643.

THE COMPONENT PART IS PROVIDED HERE TO ALLOW USERS ACCESS TO INDIVIDUALLY AUTHORED SECTIONS OF PROCEEDINGS, ANNALS, SYMPOSIA, ETC. HOWEVER, THE COMPONENT SHOULD BE CONSIDERED WITHIN THE CONTEXT OF THE OVERALL COMPILATION REPORT AND NOT AS A STAND-ALONE TECHNICAL REPORT.

THE FOLLOWING COMPONENT PART NUMBERS COMPRISE THE COMPILATION REPORT:

COMPONENT PART NOTICE (CON'T)

AD#:	TITLE:
AD-P004 269	Leistungssteigerung und Verbesserung des Fahrkomforts Bei Selbstfahrenden Baumaschienen Durch Reduzierung Einsatbedingter Nick- und Hubschwingungen (Increase in Performance and Improvement of Ride Comfort of Self-Propelled Construction Machinery by Reducing Pitch and Vertical Vibration)
AD-P004 270	Stresses in Situ Generating by Bulldozers
AD-P004 271	Finite Element Analysis of Ground Deformation Beneath Moving Track Loads
AD-P004 271	A Rig for Testing the Soft Soil Performance of Track Systems
AD-P004 273	Die Abhaengigkeit der Bodentragfaehigkeit und der Zugkraft von der Abstandgroesse der Bodenplatten (The Dependence of Soil Bearing Capacity and Drawbar Pull on the Spacing between Track Plates)
AD-P004 274	The Dynamic Interaction between Track and Soil
AD-P004 275	Analysis of Ground Pressure Distribution Beneath Tracked Model with Respect to External Loading
AD-P004 276	A Comparison between a Conventional Method and an Improved Method for Predicting Tracked Vehicle Performance
AD-P004 277	Effect of Hitch Positions on the Performance of Track/Grouser Systems
AD-P004 278	Grouser Effect Studies
AD-P004 279	Ride Comfort of Off-Road Vehicles
AD-P004 280	Further Development in Ride Quality Assessment
AD-P004 281	Comparison of Measured and Simulated Ride Comfort for an Agricultural Tractor and Influence of Travel Speed and Tyre-Inflation Pressure on Dynamic Response
AD-P004 282	Characteristics of Fram Field Profiles as Sources of Tractor Vibration

Distribution/
Availability Codes

Dist	Avail and/or Special
A-1	

DEVELOPMENT OF A SOIL-WHEEL INTERACTION MODEL

George Y. Baladi (Member, ISTVS) and Behzad Rohani
U.S. Army Engineer Waterways Experiment Station, Vicksburg, Mississippi

ABSTRACT

The development of a mathematical model for calculating the motion resistance, sinkage, drawbar pull, torque, and side force for a flexible wheel traversing a yielding (or deformable) surface is described. In order to make the problem tractable, the deformed boundary of the wheel is assumed to be an arc of a larger circular wheel. The entire soil-wheel interaction process is treated as two springs in series, one describing the flexibility of the tire and one describing the elastic-plastic deformation of the soil. Mathematical expressions are derived for the two spring constants in terms of the load deflection characteristics of the tire, the undeflected configuration of the wheel, and the mechanical properties of the soil (both shearing response and compressibility characteristics).

The system of equations describing the performance of the wheel is solved numerically via a computer program called TIRE. Using this program, a series of parametric calculations is conducted to demonstrate the application of the methodology and to study the performance of flexible wheels on different types of soil under various kinematic conditions. A partial validation of the proposed interaction model is established by comparing the results of a large number of laboratory single wheel tests on both clay and sand with the corresponding model predictions.

INTRODUCTION

The determination of the response of a single flexible wheel traversing a yielding (or deformable) surface is essential for the analysis of the steering performance of wheeled vehicles. Specifically, the sinkage, motion resistance, drawbar pull, torque, and side forces acting on a powered flexible wheel moving on a yielding soil must be accurately determined. Due to the overwhelming complexity of this problem, previous research in this area has been directed, by and large, towards extensive experimentation and the development of empirical equations relating the various parameters of the problem (Reference 1). Unfortunately, these empirical equations are not generic and apply only within the range of the experimental data on which they are based. On the other hand, most of the analytical investigations conducted in this area are based on the assumption of a rigid wheel (Reference 2). That is, the effect of the flexibility (elasticity) of the tire on the kinematics of the wheel is neglected. Even in the case of the rigid wheel, there is no general equation that can predict accurately the sinkage as a function of applied load, configuration of the wheel, and the engineering properties of soil (Reference 3). In a recent article, Fujimoto (Reference 4) introduced the flexibility of the tire in his analysis of the performance of elastic wheels on cohesive soils. He introduced an empirical relation between the central angle of the wheel, the internal pressure of the tire, and the radial stress acting on the periphery of the tire. The radial stress was assumed to be constant over the periphery of the tire. Fujimoto concluded that the determination of the radial stress is the most difficult problem in the analysis of soil-wheel interaction and recommended an empirical relation between the mobility cone index (CI) and the radial stress.

The objective of the present investigation is to develop a rational soil-wheel interaction model that is free from excessive empiricism and is general enough to treat a wide range of problems. The core of the model is a method for predicting the sinkage as a function of applied load, deflection of the tire, slip, undeformed geometry of the wheel, and the fundamental engineering properties of the soil (such as cohesion, angle of internal friction, density, compressibility, etc.). Accordingly, the model can be used to predict sinkage in sand, clay, or soils exhibiting both cohesive and frictional properties. The equilibrium conditions and the sinkage of the wheel are then combined to calculate motion resistance, drawbar pull, torque, etc.

To demonstrate the application of the proposed model, a series of parametric calculations is conducted to determine the performance of flexible wheels on different types of soil under various kinematic conditions. Also, a partial validation of the model is established by comparing the results of a large number of laboratory single wheel tests on both clay and sand with corresponding model predictions.

DERIVATION OF THE SOIL-WHEEL INTERACTION MODEL

General Procedure

The most essential part of the soil-wheel interaction model is a procedure for determining the sinkage of a flexible wheel. The basic parameters that must be included in such a procedure are the applied load, configuration of the wheel, flexibility or elasticity of the tire, slip, and the fundamental engineering properties of the soil (such as shear strength and compressibility). The development of the physical soil-wheel interaction model is presented in detail in the subsequent sections and is based on the assumption that the entire interaction process can be simulated by two springs in series, with one spring defining the elasticity of the tire and the other describing the elastic-plastic deformation of the soil. These two springs are then combined into a single equivalent spring describing the interaction of the soil-wheel system.

The simulation of the resistance of the soil by a spring constant leads to a nonuniform distribution of normal stresses at the soil-wheel interface. The shear stresses at the soil-wheel interface are calculated from a rheological model which describes the shearing stress-strain characteristics of the soil. The final step of the analyses is to determine the motion resistance, drawbar pull, torque, efficiency, and side force for a flexible wheel traversing a yielding surface. These parameters are calculated based on the assumption that the deformed boundary of the tire is an arc of a larger circular wheel.

Spring Constant for a Flexible Tire

A typical load-deflection curve for a flexible tire on a rigid surface is shown in Figure 1 where Δ denotes the deflection of the tire at point A. In practice, Δ is usually expressed as a percentage of the unloaded section height of the tire (Figure 2). The radial deflection of a generic point B along the periphery of the tire at an angle α is specified by Δ_α (Figure 1). If the deformed section of the tire is characterized by a continuous spring with constant k_t, then the vertical differential force dF applied at point B can be expressed as

$$dF = k_t \, \Delta_\alpha \cos\alpha \, d\alpha \quad \ldots \quad (1)$$

From Figure 1, Δ_α can be expressed in terms of Δ, α, and the undeflected radius of the wheel R

$$\Delta_\alpha = R - \frac{R - \Delta}{\cos\alpha} = \frac{R}{\cos\alpha}\left[\cos\alpha - \left(1 - \frac{\Delta}{R}\right)\right] \quad \ldots \quad (2)$$

Substitution of Equation 2 into Equation 1 leads to

$$dF = Rk_t\left[\cos\alpha - \left(1 - \frac{\Delta}{R}\right)\right] d\alpha \quad \ldots \quad (3)$$

Also, from Figure 1,

$$\cos\frac{\theta_t}{2} = 1 - \frac{\Delta}{R} \quad \ldots \quad (4)$$

In view of Equations 3 and 4 and static equilibrium, the applied load W can be expressed as

$$W = 2\int_0^{\frac{\theta_t}{2}} dF = 2Rk_t \int_0^{\frac{\theta_t}{2}} \left(\cos\alpha - \cos\frac{\theta_t}{2}\right) d\alpha \quad \ldots \quad (5)$$

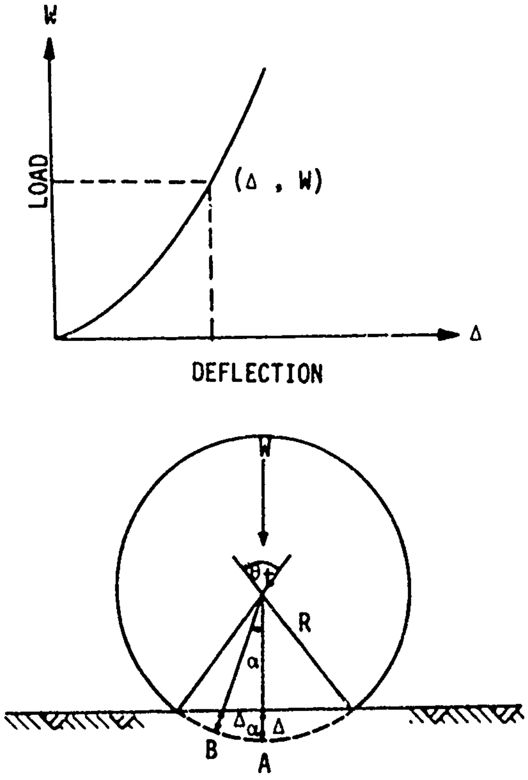

Figure 1. Load-deflection curve for a flexible tire on a rigid surface

1. UNLOADED SECTION WIDTH (D)
2. UNLOADED RADIUS (R)
3. UNLOADED SECTION HEIGHT (h)
4. DEFLECTION AT GIVEN LOAD = Δ/h

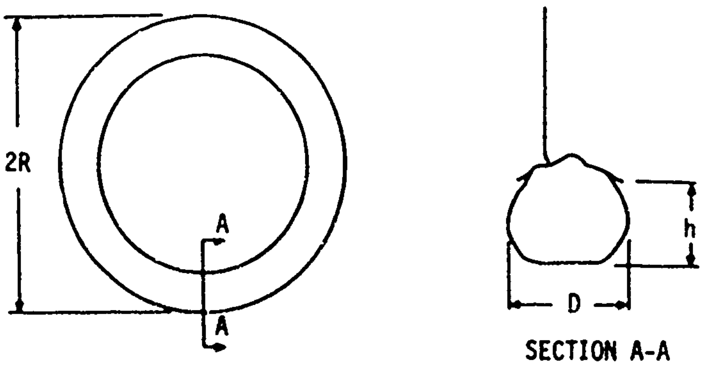

Figure 2. Tire geometry

Integration of Equation 5 leads to the following relation for the spring constant k_t

$$k_t = \frac{W}{2R\left(\sin\frac{\theta_t}{2} - \frac{\theta_t}{2}\cos\frac{\theta_t}{2}\right)} \quad (6)$$

The spring constant k_t can also be expressed in terms of Δ by combining Equations 4 and 6:

$$k_t = \frac{W}{2\Delta\left[\sqrt{\frac{2R}{\Delta} - 1} - \left(\frac{R}{\Delta} - 1\right)\cos^{-1}\left(1 - \frac{\Delta}{R}\right)\right]} \quad (7)$$

Equation 7 is portrayed in the top of Figure 1.

Spring Constant for Soil

Let σ_c be the radial stress necessary to maintain a slow expansion of a spherical cavity in an elastic-plastic medium from radius R_o to R (Figure 3a). The radial stress σ_c is expressed analytically in terms of the shear strength parameters and the volume change characteristics of soil (Reference 5). The resistance of the soil to expansion of the spherical cavity can be simulated by a continuous spring characterized by spring constant k_s. From Figure 3a, the spring constant k_s can be expressed as

$$k_s = \frac{\pi\left(R^2 - R_o^2\right)\sigma_c}{R - R_o} = \pi\left(R + R_o\right)\sigma_c \quad (8)$$

where $R - R_o$ corresponds to spring deflection. Now consider a wheel of radius R embedded in soil to a depth $R - R_o$ (Figure 3b). The normal stress at point A resisting the embedment of the wheel is assumed to be equal to the radial stress σ_c inside the expanding cavity. Similar to expansion of the spherical cavity (Figure 3a), the resistance of the soil to the embedment of the wheel can also be simulated by a continuous spring with constant k_s given by

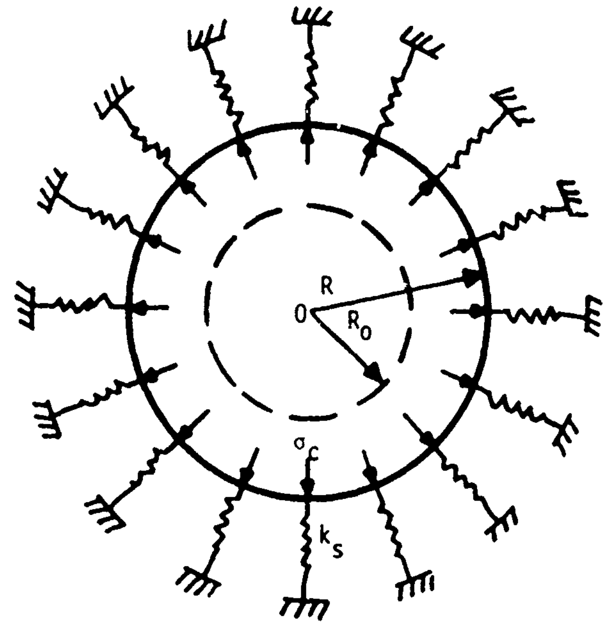

a. EXPANSION OF SPHERICAL CAVITY

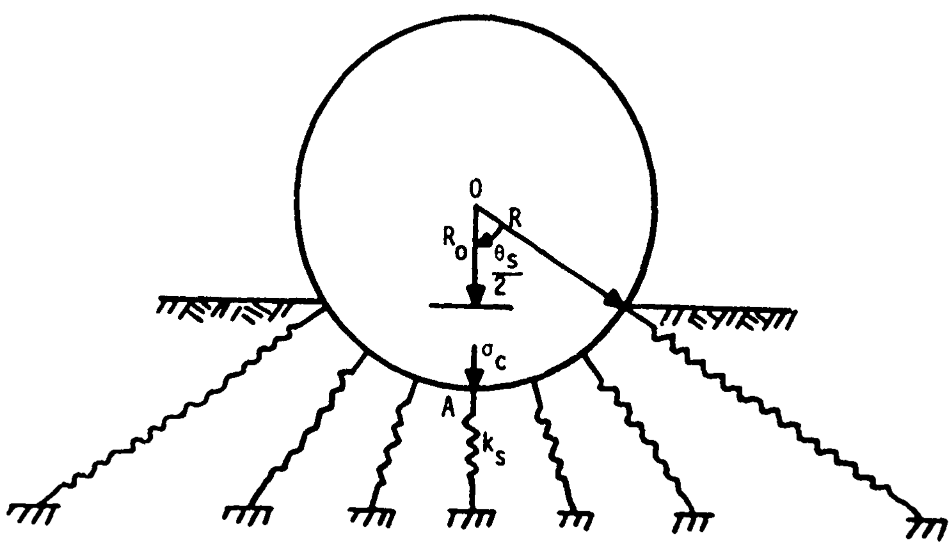

b. ANALOGY BETWEEN A WHEEL EMBEDDED IN SOIL AND CAVITY EXPANSION PROBLEM

Figure 3. Proposed model for computing the spring constant for soil

$$k_s = \frac{RD}{R - R_o} \sigma_c \quad \text{(9)}$$

where D is the unloaded section width of the wheel (Figure 2). Combining Equations 8 and 9 we obtain

$$\frac{\pi\left(R + R_o\right)\left(R - R_o\right)}{RD} = 1 \quad \text{(10)}$$

where, from Figure 3b

$$R + R_o = R\left(1 + \cos\frac{\theta_s}{2}\right) \quad \text{(11)}$$

$$R - R_o = R\left(1 - \cos\frac{\theta_s}{2}\right) \quad \text{(12)}$$

Substituting Equations 11 and 12 into Equation 10 and solving for $\cos \theta_s/2$ and θ_s, we obtain

$$\cos\frac{\theta_s}{2} = \sqrt{1 - \frac{D}{\pi R}} \quad \text{(13)}$$

$$\theta_s = 2\cos^{-1}\sqrt{1 - \frac{D}{\pi R}} \quad \text{(14)}$$

Substitution of Equations 11 and 13 into Equation 8 leads to the following expression for the spring constant k_s :

$$k_s = \pi R\left(1 + \sqrt{1 - \frac{D}{\pi R}}\right)\sigma_c \quad \text{(15)}$$

It is clear from Equation 15 that the apparent spring constant of the soil is a function of the engineering properties of soil through σ_c and the geometry of the tire.

<u>Equivalent Spring Constant for the Soil-Tire System</u>

The model of the soil-tire system in terms of the spring constants k_t and k_s is portrayed in Figure 4. The equivalent spring constant k_e for

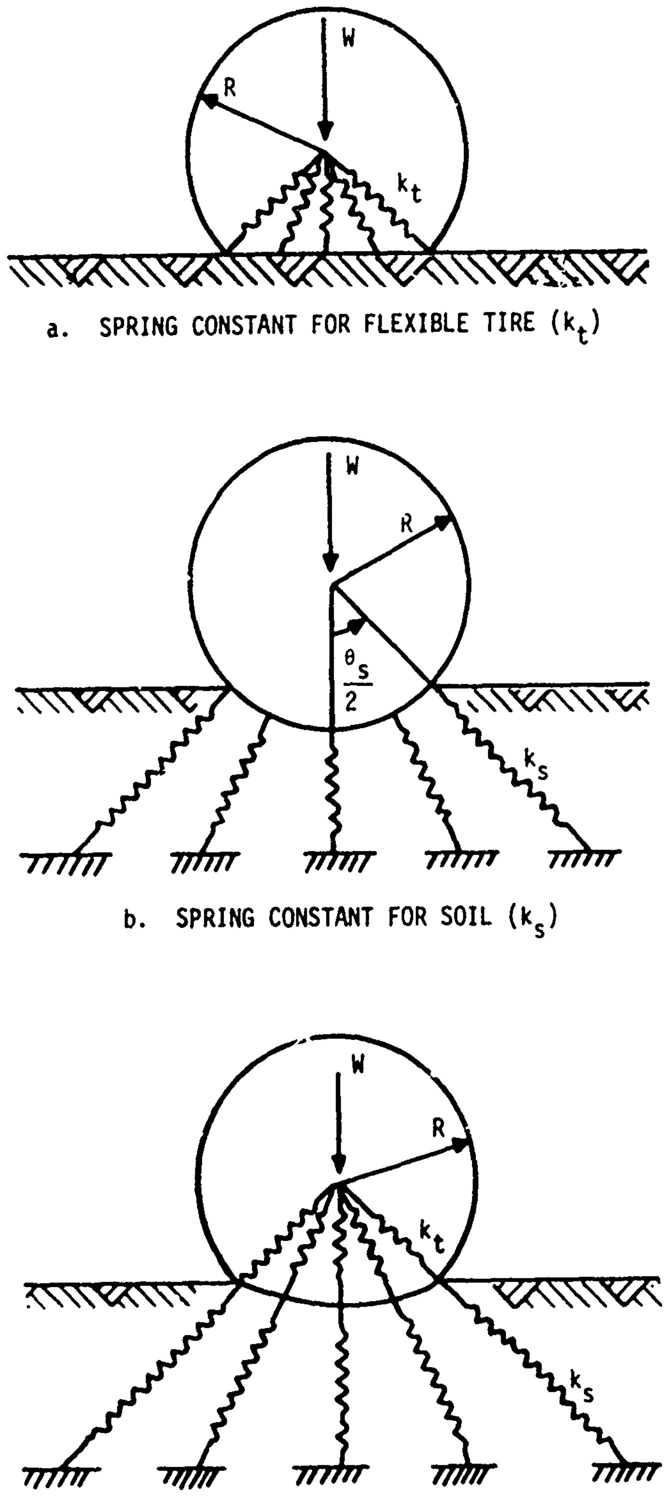

c. SPRING CONSTANT FOR SOIL-TIRE SYSTEM $\frac{k_s\, k_t}{k_s + k_t}$

Figure 4. Equivalent spring constant for soil-tire system

the soil-tire system can be determined from static equilibrium and is given as

$$k_e = \frac{k_t\ k_s}{k_s + k_t} \quad \ldots\ldots\ldots\ldots\ldots\ldots\ldots\ldots\ldots\ldots \quad (16)$$

Normal and Shear Stress Distributions at the Soil-Tire Interface

Based on the concept of the spring analogy advanced in the previous sections, the expression for differential vertical force at a generic point at the soil-tire interface can be expressed as (Figure 5)

$$dF = DR\sigma_N \cos\left(\alpha + \frac{\theta}{2}\right) d\alpha = \frac{k_s\ R\left(\cos\alpha - \cos\frac{\theta}{2}\right)\cos\left(\alpha + \frac{\theta}{2}\right)d\alpha}{\cos\alpha} \quad \ldots\ldots \quad (17)$$

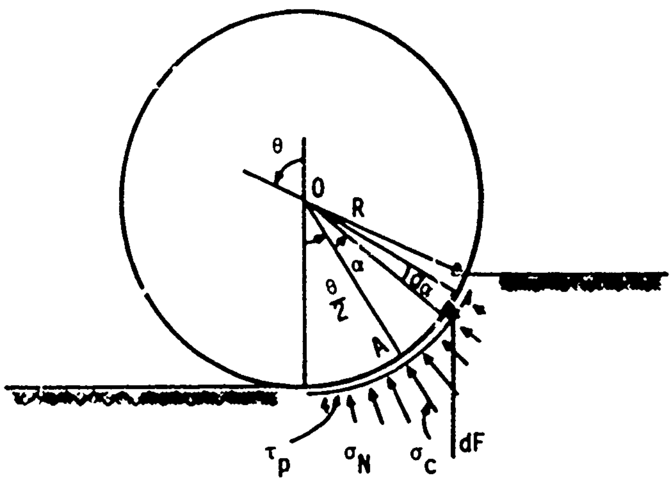

Figure 5. Normal stress distribution along the soil-tire interface

Solving Equation 17 for σ_N, we obtain

$$\sigma_N = \frac{k_s\left(\cos\alpha - \cos\frac{\theta}{2}\right)}{D\ \cos\alpha} \quad \ldots\ldots\ldots\ldots\ldots\ldots\ldots\ldots \quad (18)$$

In view of Equations 9 and 12, Equation 18 becomes

$$\sigma_N = \frac{\left(\cos\alpha - \cos\frac{\theta}{2}\right)\sigma_c}{\left(1 - \cos\frac{\theta}{2}\right)\cos\alpha} \quad \ldots \ldots \ldots \ldots \ldots \ldots \quad (19)$$

Equation 19 describes the distribution of normal stress σ_N at the soil-tire interface. Note that at point A (Figure 5) where $\alpha = 0$, Equation 19 indicates that $\sigma_N = \sigma_c$, which is consistent with the assumption made in the previous sections. On the other hand, at the free surface where $\alpha = \pm\theta/2$ (Figure 5) Equation 19 indicates that $\sigma_N = 0$ at these points.

Consider now a tire with turn angle η with respect to the direction of motion. The plan view of the tire is shown in Figure 6a. If slip in the plane of the wheel is defined by the slip ratio S , then slip in the direction of the motion can be expressed as

$$S_m = \frac{S}{\cos\eta} \quad \ldots \ldots \ldots \ldots \ldots \ldots \quad (20)$$

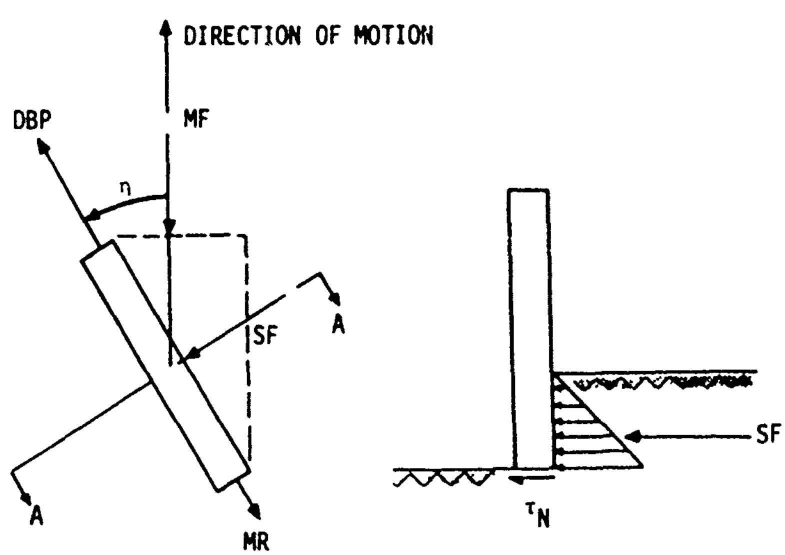

a. PLAN VIEW

b. STRESS DISTRIBUTION ALONG SECTION AA

Figure 6. Geometry of the tire with turn angle η

The components of shear stress parallel and perpendicular to the plane of the wheel τ_p and τ_N , respectively, can be obtained from the rheological soil model presented in Reference 5.

Combining Equation 20 with the rheological soil model results in the following expressions for τ_p and τ_N

$$\tau_p = \frac{G\left(C + \sigma_N \tan\phi\right)S}{\left|\frac{GS}{\cos\eta}\right| + C + \sigma_N \tan\phi} \qquad (21)$$

$$\tau_N = \frac{G\left(C + \sigma_N \tan\phi\right)S \tan\eta}{\left|\frac{GS}{\cos\eta}\right| + C + \sigma_N \tan\phi} \qquad (22)$$

where σ_N is given by Equation 19. In Equations 21 and 22, G, C, and ϕ correspond, respectively, to shear modulus, cohesion, and angle of internal friction of the material.

Deflection and Sinkage of a Flexible Tire

If the deflection of a flexible tire on a rigid surface under a given load W is denoted by Δ (Figure 1), then the corresponding deflection on a yielding soil Δ_t (Figure 7b) can be determined from the concept of the equivalent spring constant

$$\Delta_t = \frac{k_s}{k_s + k_t}\Delta \qquad (23)$$

Similarly, if Z_r is the sinkage of a rigid wheel under a given load W (Figure 7c), then the corresponding sinkage Z of a flexible wheel (Figure 7b) is

$$Z = \left(\frac{k_t}{k_s + k_t}\right)Z_r \qquad (24)$$

The sinkage Z_r can be calculated from the balance of forces in the vertical direction (Figure 8a)

$$W = DR \int_{-\frac{\theta_1}{2}}^{\frac{\theta_1}{2}} \left[\sigma_N \cos\left(\alpha + \frac{\theta_1}{2}\right) + \tau \sin\left(\alpha + \frac{\theta_1}{2}\right)\right] d\alpha \qquad (25)$$

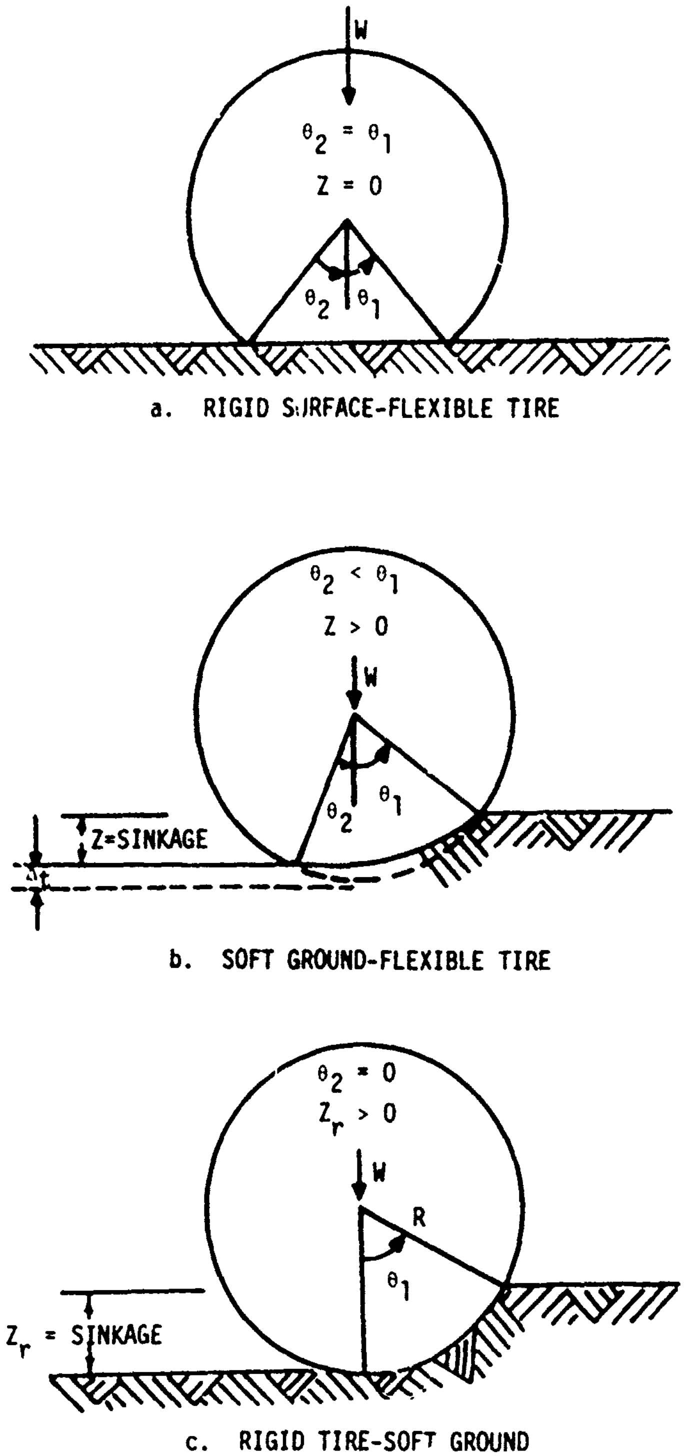

Figure 7. Variation of the central angles θ_1 and θ_2 and sinkage Z with relative rigidity of the tire and soil

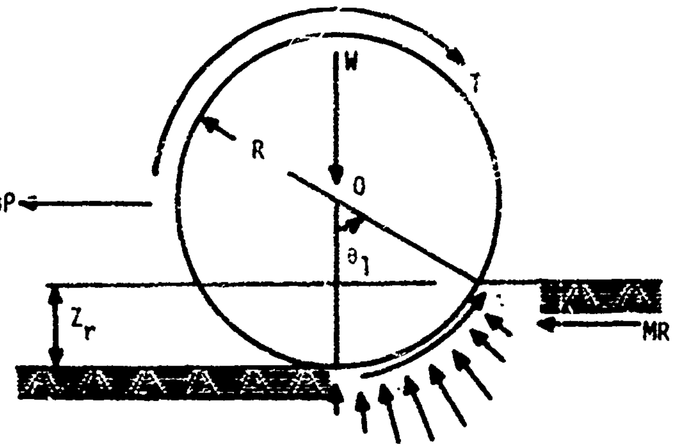

a. SINKAGE OF A RIGID WHEEL

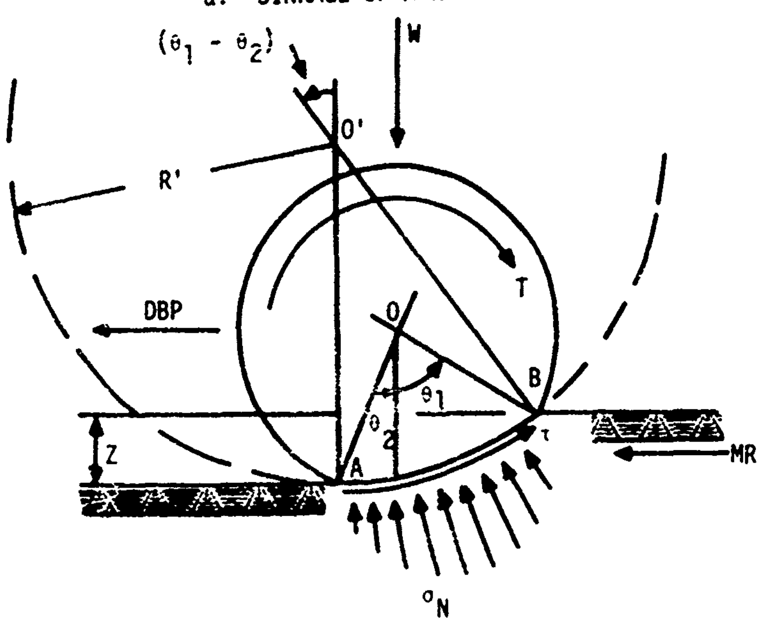

b. SINKAGE OF A FLEXIBLE WHEEL

Figure 8. Geometry of the problem

where σ_N is given by (see Equation 19)

$$\sigma_N = \frac{\left(\cos\alpha - \cos\frac{\theta_1}{2}\right)\sigma_c}{\left(1 - \cos\frac{\theta_1}{2}\right)\cos\alpha} \quad \ldots\ldots\ldots \quad (26)$$

The shear stress τ in Equation 25 can be obtained from the rheological soil model described in Reference 5 and has the following form

$$\tau = \frac{G\left(C + \sigma_N \tan\phi\right)S}{|GS| + C + \sigma_N \tan\phi} \quad \ldots \quad (27)$$

where σ_N is given by Equation 26. The solution of Equation 25 leads to an expression for θ_1. The actual sinkage Z_r can then be calculated from (Figure 7c)

$$Z_r = R\left(1 - \cos\theta_1\right) \quad \ldots \quad (28)$$

Relationships Governing Single Wheel Performance

Geometry of the problem

Consider the geometry and boundary conditions for a flexible wheel-soil system shown in Figure 8b. The contact surface between the wheel and the soil is assumed to be an arc of a circle with a radius equal to or larger than the undeflected radius of the wheel (only in the case of the rigid wheel is the radius equal to the undeflected radius). The center of this circle O' is located at the intersection of the vertical line through point A and the bisector of the angle $\hat{AOB}$. According to Figure 7b, the relationship between the angle θ_1, the sinkage Z, and the deflection of the tire Δ_t is

$$\theta_1 = \cos^{-1}\left(1 - \frac{Z}{R} - \frac{\Delta_t}{R}\right) \quad \ldots \quad (29)$$

Also, from the geometry of Figure 7b

$$\theta_2 = \cos^{-1}\left(1 - \frac{\Delta_t}{R}\right) \quad \ldots \quad (30)$$

From the geometry of Figure 8b

$$R' = \frac{Z}{1 - \cos\left(\theta_1 - \theta_2\right)} \quad \ldots \quad (31)$$

Using Equations 29 and 30 to eliminate Z from Equation 31, we obtain the following relation for R' in terms of R and the central angles θ_1 and θ_2

$$R' = R \frac{\sin \frac{\theta_1 + \theta_2}{2}}{\sin \frac{\theta_1 - \theta_2}{2}} \quad \text{. . . . .} \quad (32)$$

Equations 29 through 32 completely define the shape of the contact surface between the soil and the tire.

Tire internal motion resistance

The internal motion resistance (IMR) of the tire is expressed in terms of the deflection of the tire on a rigid surface. Data from a number of experiments where IMR has been measured are portrayed in Figure 9 (Reference 6), which shows that IMR increases rapidly with deflection. The dashed curves in Figure 9 are approximate upper and lower bounds to the

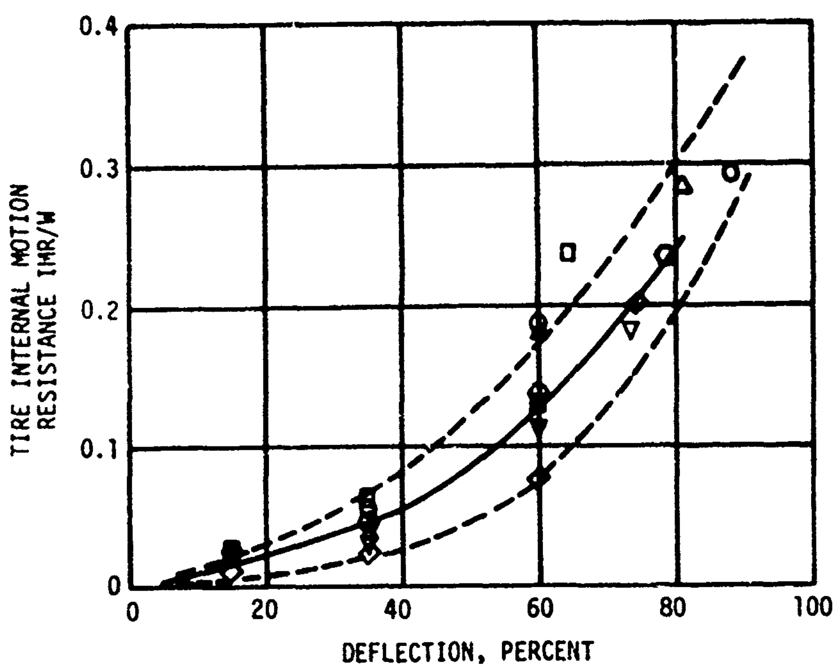

Figure 9. Tire internal motion resistance-deflection relation (Reference 6)

test data. The solid curve in Figure 9 may be viewed as the average response and is fitted with the following mathematical expression for calculations of internal motion resistance:

$$IMR = \left[4\left(\frac{\Delta}{h}\right)^2 + 0.2\left(\frac{\Delta}{h}\right)\right]\frac{W}{10} \quad \ldots \quad (33)$$

Motion resistance, drawbar pull, torque, efficiency and side force

We can now proceed to develop appropriate equations for motion resistance (MR), drawbar pull (DBP), torque (T), and efficiency (E). From Figures 6 and 8b

$$MR = R'D \int_{-\frac{(\theta_1-\theta_2)}{2}}^{\frac{(\theta_1-\theta_2)}{2}} \sigma_N \sin\left(\alpha + \frac{\theta_1-\theta_2}{2}\right) d\alpha + IMR + MF\cos\eta \quad \ldots \quad (34)$$

$$DBP = R'D \int_{-\frac{(\theta_1-\theta_2)}{2}}^{\frac{(\theta_1-\theta_2)}{2}} \tau_p \cos\left(\alpha + \frac{\theta_1-\theta_2}{2}\right) d\alpha - MR \quad \ldots \quad (35)$$

$$T = R'D \int_{-\frac{(\theta_1-\theta_2)}{2}}^{\frac{(\theta_1-\theta_2)}{2}} \tau_p \left(R' - \frac{R\sin\theta_2}{\sin\frac{\theta_1-\theta_2}{2}}\cos\alpha\right) d\alpha \quad \ldots \quad (36)$$

$$E = \frac{DBP}{T}(1 - S)\left(R - \Delta_t\right) \quad \ldots \quad (37)$$

where σ_N and τ_p are given by Equations 19 and 21, respectively, with θ replaced by $\theta_1 - \theta_2$, and $MF = R^2\left(\theta_1 - \frac{\sin 2\theta_1}{2}\right)\sigma_c \sin\eta$. Similarly, from Figures 6 and 8 the side force (SF) is

$$SF = R'D \int_{-\frac{(\theta_1-\theta_2)}{2}}^{\frac{(\theta_1-\theta_2)}{2}} \tau_N \, d\alpha + MR \tan\eta \quad \ldots\ldots\ldots\ldots \quad (38)$$

where τ_N is given by Equation 22. The above system of equations provides a complete solution to the performance of a flexible tire traversing a yielding soil. A computer program called TIRE has been developed which numerically solves the above system of equations.

PARAMETRIC STUDIES OF THE PERFORMANCE OF A FLEXIBLE WHEEL ON A YIELDING SOIL

In this part, the performance of a flexible wheel on both clay soil and sand is parametrically investigated (for $\eta = 0$). In addition, the effects of the unloaded section width, the deflection of the tire, and the slip ratio on the performance of the wheel are also analyzed. The radius of the flexible wheel used for the central case is 14.1 in., its width is 8.28 in., and its carcass section height is 6.35 in. All calculations were conducted for an applied wheel load of 1000 lbs. The results of the parameter study are presented in the following sections.

Sinkage

The results of the calculations for assessing the effect of soil type, slip ratio, and tire deflection on sinkage are presented in Figures 10 through 13. Figures 10 and 12 indicate that for both clay soil and sand sinkage increases with increasing slip ratio. The effect of tire deflection on sinkage is portrayed in Figures 11 and 13 for clay and sand, respectively. As indicated in these figures, the sinkage decreases rapidly with increasing tire deflections from zero (rigid wheel) up to approximately 40 percent deflection. Beyond 40 percent deflection, the rate of decrease in sinkage is small.

Motion Resistance

The effects of soil type, slip ratio, and tire deflection on motion resistance are shown in Figures 14 through 17. Figures 14 and 16 indicate that

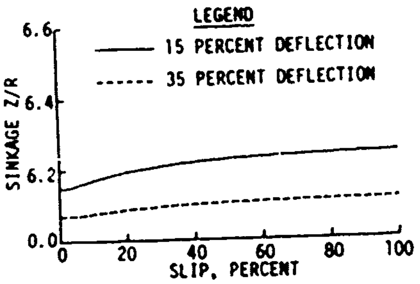

Figure 10. Relationship between sinkage and slip ratio for clay

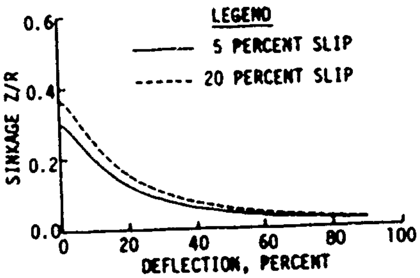

Figure 11. Relationship between sinkage and tire deflection for clay

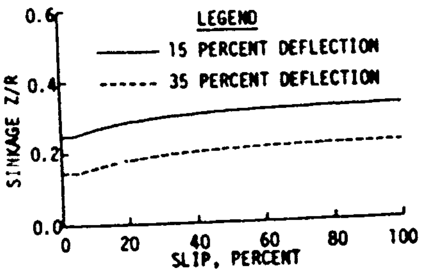

Figure 12. Relationship between sinkage and slip ratio for sand

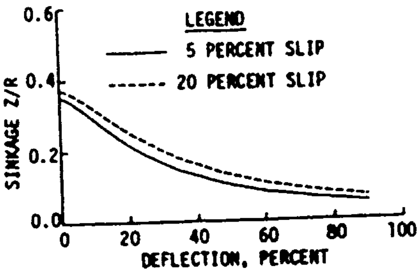

Figure 13. Relationship between sinkage and tire deflection for sand

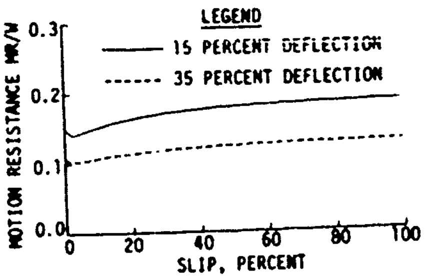

Figure 14. Relationship between motion resistance and slip ratio for clay

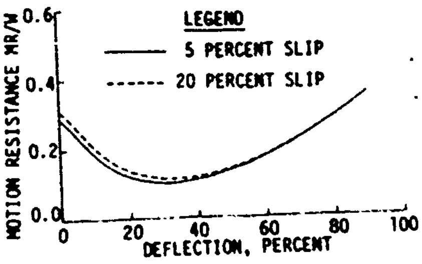

Figure 15. Relationship between motion resistance and tire deflection for clay

motion resistance initially decreases with increasing slip ratio up to a slip ratio of approximately 4 percent and increases thereafter. This initial decrease in motion resistance has been observed experimentally and is attributed to the plowing action of the tire. The increase in motion resistance at higher slip ratios is due to an increase in sinkage (see Figures 10 and 12). Relationships between motion resistance and tire deflection for each soil type studied are shown in Figures 15 and 17. The motion resistance initially decreases with increasing tire deflection and reaches a minimum value at about 30 percent deflection. At tire deflections higher than 30 percent, the motion resistance increases again. The initial decrease in motion resistance can be attributed to the initial rapid decrease in sinkage (see Figures 11 and 13). The increase in motion resistance at deflections larger than 40 percent is due to a rapid increase in the internal motion resistance of the tire (see Figure 9).

Drawbar Pull

Figures 18 through 21 portray the effects of soil type, slip ratio, and tire deflection on drawbar pull. Figure 18 indicates that for clay soil the drawbar pull increases rapidly for slip ratios between zero and about 10 percent. For higher slip ratios, the increase in drawbar pull is relatively small. For sand, on the other hand, the drawbar pull increases rapidly and reaches a peak value at about 20 percent slip ratio (Figure 20). The drawbar pull then drops for slip ratios in the range of about 20 to 50 percent. Beyond 50 percent slip ratio, the drawbar pull increases very slowly. This type of behavior also has been observed experimentally. Relationships between drawbar pull and tire deflection for each type of soil studied are presented in Figures 19 and 21. As indicated in Figures 19 and 21, the drawbar pull initially increases with deflection up to a deflection of approximately 50 percent. Beyond this deflection, the drawbar pull decreases because of a rapid increase in the internal motion resistance of the tire (see Figure 9).

Effect of Section Width on Tire Performance

Figures 22 through 25 present the effect of the unloaded section width on sinkage, motion resistance, drawbar pull, and torque, respectively, for clay soil at 15 percent tire deflection. Figure 22 shows that sinkage decreases rapidly as tire width increases from approximately D/R = 0.2 to

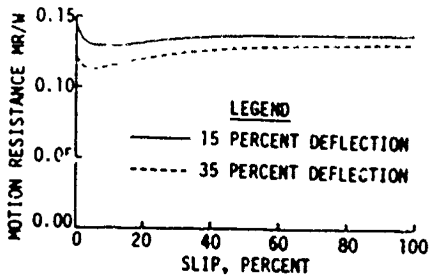

Figure 16. Relationship between motion resistance and slip ratio for sand

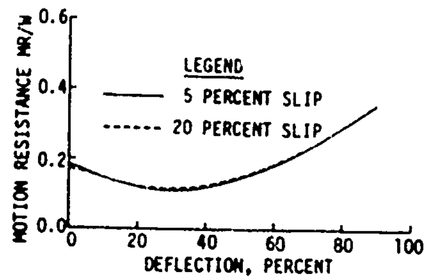

Figure 17. Relationship between motion resistance and tire deflection for sand

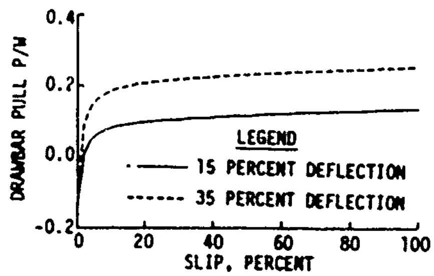

Figure 18. Relationship between drawbar pull and slip ratio for clay

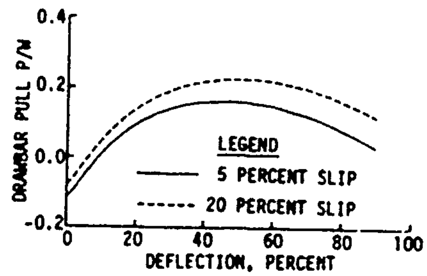

Figure 19. Relationship between drawbar pull and tire deflection for clay

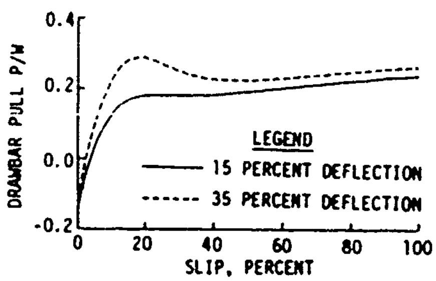

Figure 20. Relationship between drawbar pull and slip ratio for sand

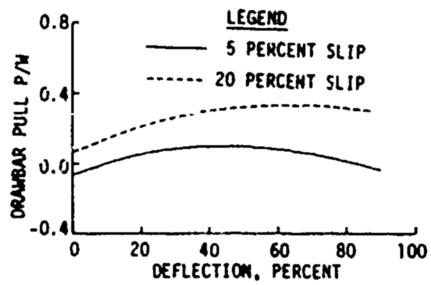

Figure 21. Relationship between drawbar pull and tire deflection for sand

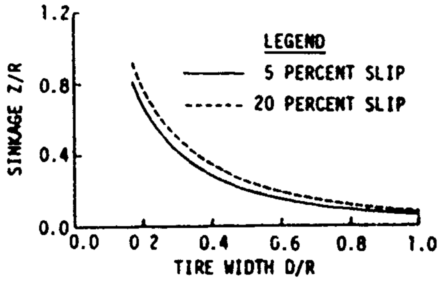

Figure 22. Relationship between sinkage and tire width for clay; 15 percent tire deflection

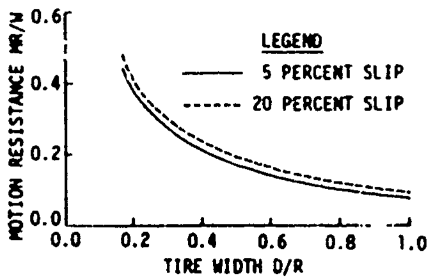

Figure 23. Relationship between motion resistance and tire width for clay; 15 percent tire deflection

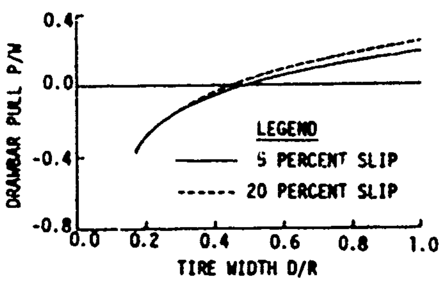

Figure 24. Relationship between drawbar pull and tire width for clay; 15 percent tire deflection

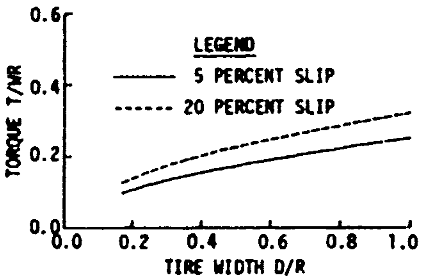

Figure 25. Relationship between torque and tire width for clay; 15 percent tire deflection

D/R = 0.5. For larger tire widths the decrease in sinkage is relatively small. Figure 23 shows that the motion resistance decreases as the width of the tire increases. This is expected because as the width of the tire increases, the sinkage decreases (see Figure 22). It should be pointed out that in Figure 23 the internal motion resistance of the tire was assumed to be independent of the width of the tire. If the effect of width on the internal motion resistance of the tire were taken into consideration, the result in Figure 23 would have been different.

Figure 24 indicates that the drawbar pull increases as the tire width increases. Most of the increase in the drawbar pull takes place for the tire widths less than 50 percent of the radius. For larger tire widths, the rate of increase in drawbar pull is relatively small. This behavior is also related to sinkage (Figure 22), where it is observed that most of the decrease in sinkage takes place for tire widths less than 50 percent of the radius. The relationship between torque and tire width is shown in Figure 25. The trend in Figure 25 is similar to Figure 24.

CORRELATION OF TEST DATA WITH MODEL PREDICTIONS

Background

The results of the extensive parameter studies presented in the previous section indicated that the model predictions are qualitatively in agreement with the observed performance of flexible wheels on a yielding soil. A detailed quantitative validation of the proposed model requires controlled laboratory tests and the measurement of the appropriate soil properties discussed in Reference 5. A partial validation of the model, however, can be accomplished by using test data already documented in the literature. The main drawback in using existing data from the literature is the lack of information on the mechanical properties of the soil used in the experiment. Usually the soil is characterized in terms of simple indices such as the mobility cone index (CI). These indices must be translated to the appropriate soil properties required by the proposed model. This is not an easy task and requires a separate analysis (divorced from the soil-wheel interaction model) to make such a translation. Usually one is forced to determine the numerical values of several material constants from an index such as the CI. This inherently introduces uncertainties (or a bias) in the numerical values of the constants which, of course, will affect the degree of correlation between the model predictions and the test data. In spite of such uncertainties, a partial validation of the proposed soil-wheel interaction model is attempted for the zero turn angle.

Test Parameters

Test data for 13 different tires and 2 soil types (clay and sand) were selected from the literature for correlation with model predictions (Reference 1). The D/R of the test tires ranged from 0.122 (bicycle tire) to 1.737. A total of 165 data points was selected (65 test data for clay and 100 for sand) for different wheel loads and tire deflections. The tests, however, were all conducted at 20 percent slip. Soil data for all the tests were given in terms of the mobility cone index (CI). Using a methodology developed in Reference 7, the appropriate soil properties required by the model were estimated from the CI data. A summary of all the test data and the companion soil properties are given in Reference 5 and for the sake of brevity are not included in this paper.

Model Predictions

The results of model predictions are plotted against the corresponding test data in Figures 26 through 31 for sinkage, drawbar pull, and torque. Each figure contains a 45-degree line (line of perfect correlation), a line of least square fit, and the standard deviation σ which signifies the deviation between the experimental data and the corresponding model predictions. It is a measure of the deviation of the data points in the figures from the line of perfect correlation. Comparisons between the least square lines and the 45-degree lines indicate that the overall correlation of the model predictions with the test data is very reasonable in spite of two possible sources of error--that is, the general scatter in the test data and the uncertainty in estimating several soil properties from a single cone index. The sinkage, which is one of the most difficult parameters to predict, has the lowest standard deviation. The degree of correlation exhibited between the test results and model predictions indicates that the physical basis of the proposed soil-wheel interaction model is sound for both cohesive soils and granular materials. Therefore, it may be concluded that the proposed model is capable of simulating the interaction

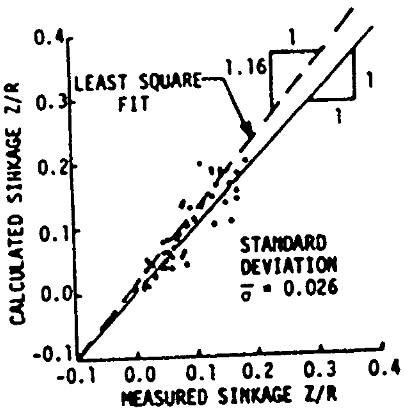

Figure 26. Predicted versus measured sinkage for clay

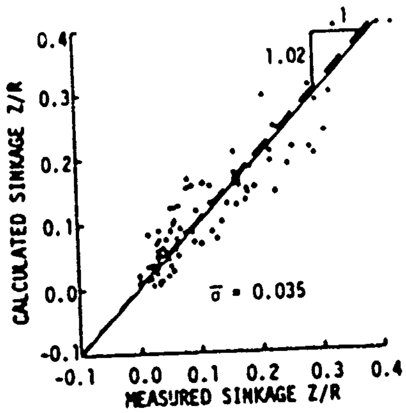

Figure 27. Predicted versus measured sinkage for sand

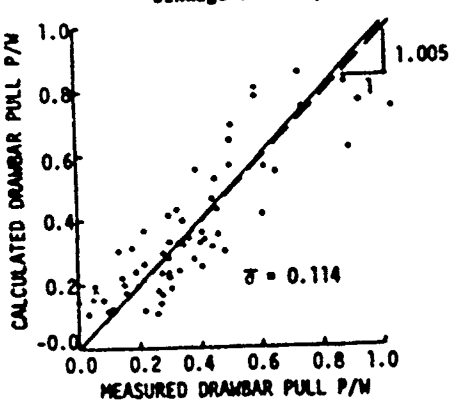

Figure 28. Predicted versus measured drawbar pull for clay

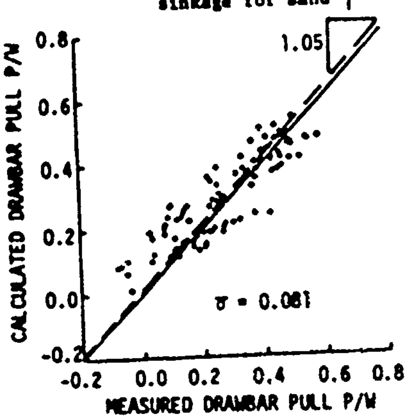

Figure 29. Predicted versus measured drawbar pull for sand

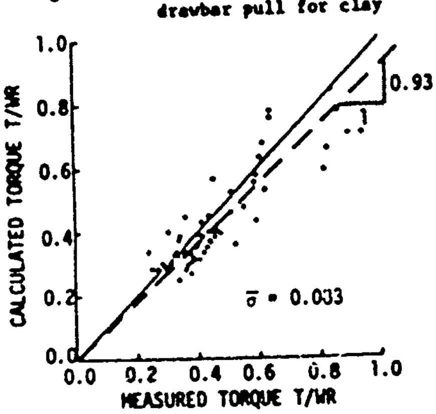

Figure 30. Predicted versus measured torque for sand

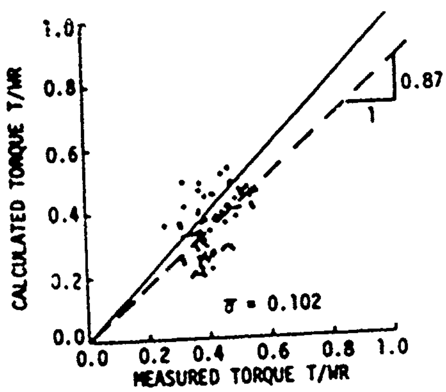

Figure 31. Predicted versus measured torque for sand

between a flexible tire and a soil exhibiting both cohesive and frictional properties.

SUMMARY AND CONCLUSIONS

A mathematical model for calculating the motion resistance, sinkage, drawbar pull, torque, and side force of a flexible wheel traversing a yielding soil has been developed and computerized for numerical application. The entire soil-wheel interaction process was treated as two springs in series, one describing the flexibility of the tire and the other describing the strength of the soil. Mathematical expressions were derived for the two spring constants in terms of the load-deflection characteristics of the tire, the undeflected configuration of the wheel, and the mechanical properties of the soil. The motion resistance, drawbar pull, torque, efficiency, and side force for the flexible wheel were obtained from the equilibrium equations by assuming that the deformed boundary of the tire is an arc of a circle with a radius equal to or greater than the undeflected radius of the wheel. The model is partially validated by comparing the results of a large number of laboratory test data for single tires on both clay and sand with the corresponding model predictions. Efforts are presently underway at WES to couple the soil-wheel interaction model with the dynamic equilibrium equations of multi-axle wheeled vehicles for analysis of the steering performance of such vehicles.

ACKNOWLEDGEMENT

The work reported herein was conducted at the U. S. Army Engineer Waterways Experiment Station under the sponsorship of the Office, Chief of Engineers, Department of the Army, as part of Project 4A161102AT22, "Dynamic Soil-Track Interactions Governing High-Speed Combat Vehicle Performance."

The authors are grateful to Mr. Clifford J. Nuttall, Jr., for providing valuable insight during the course of this study. The efforts of Mr. Donald E. Barnes in assisting in the numerical calculations and Ms. Bobbie B. Morrow in typing the paper are appreciated.

REFERENCES

1. Turnage, G. W. 1972. "Performance of Soils Under Tire Loads; P nort 8; Application of Test Results to Tire Selection for Off-Road Vehicles," Technical Report 3-666, U. S. Army Engineer Waterways Experiment Station, CE, Vicksburg, Miss.

2. Wcng, J. and Reece, A. R. 1967. "Prediction of Rigid Wheel Performance Based on the Analysis of Soil-Wheel Stresses," Journal of Terramechanics, Vol 4, No. 1.

3. Hvorslev, M. J. 1970. "The Basic Sinkage Equations and Bearing Capacity Theories," Technical Report M-70-1, U. S. Army Engineer Waterways Experiment Station, CE, Vicksburg, Miss.

4. Fujimoto, Y. 1977. "Performance of Elastic Wheels on Yielding Cohesive Soils," Journal of Terramechanics, Vol 14, No. 4.

5. Baladi, G. Y., Rohani, B., and Barnes, D. E. 1984. "Steerability Analysis of Multi-Axle Wheeled Vehicles; Report 1; Development of a Soil-Wheel Interaction Model" Technical Report GL-84-1, U. S. Army Engineer Waterways Experiment Station, CE, Vicksburg, Miss.

6. Turnage, G. W. 1976. "In-Soil Tractive Performance of Selected Radial and Bias-Ply Tires," Paper 76-1520, The 1976 Annual Meeting of the American Society of Agricultural Engineers, Chicago, Ill.

7. Rohani, B. and Baladi, G. Y. 1981. "Correlation of Mobility Cone Index with Fundamental Engineering Properties of Soil," Miscellaneous Paper SL-81-4, U. S. Army Engineer Waterways Experiment Station, CE, Vicksburg, Miss.

NOTATION

C	Cohesion
D	Unloaded section width of the tire
DBP	Drawbar pull applied on the tire
dF	Vertical differential force
E	Efficiency of the tire
G	Shear modulus
h	Unloaded section height
IMR	Internal motion resistance of the tire
k_e	Equivalent spring constant for soil-tire system
k_s	Spring constant of the soil
k_t	Spring constant of the tire
MF	Motion resistance in the direction of motion
MR	Motion resistance in the plane of the tire
R	Radius of the tire

R_o Initial radius of an expanded cavity

R' Radius of a circle containing the deflected portion of the wheel

S Slip of the wheel in the plane of the wheel

SF Side force Applied on the tire

S_m Slip of the wheel in the direction of motion

T Torque applied on the tire

W Tire load

Z Sinkage of a flexible wheel

Z_r Sinkage of a rigid wheel

α Generic angle

Δ Maximum deflection of the tire on a hard surface

Δ_t Maximum deflection of the tire on a yielding soil

Δ_α Deflection of the tire at the generic point

η Angle between the direction of motion and the plane of the wheel

θ_t $2\cos^{-1}\left(1 - \frac{\Delta}{R}\right)$

θ_s $2\cos^{-1}\left(\frac{R_o}{R}\right) = 2\cos^{-1}\sqrt{1 - \frac{D}{R}}$

θ_1 $\cos^{-1}\left(1 - \frac{Z + \Delta_t}{R}\right)$

θ_2 $\cos^{-1}\left(1 - \frac{\Delta_t}{R}\right)$

σ_c Radial stress inside a cavity

σ_N Normal stress at the soil-tire interface

τ Shear stress at the soil-tire interface

τ_N Shear stress perpendicular to the plane of the wheel

τ_p Shear stress in the plane of the wheel

ϕ Angle of internal friction